Archives of Biochemistry and Biophysics 591 (2016) 66–75

Contents lists available at ScienceDirect

Archives of Biochemistry and Biophysics

journal homepage: www.elsevier.com/locate/yabbi

Epoxide hydrolase-catalyzed enantioselective conversion of *trans*-stilbene oxide: Insights into the reaction mechanism from steady-state and pre-steady-state enzyme kinetics

Alain Archelas [a], Wei Zhao [a], Bruno Faure [a], Gilles Iacazio [a], Michael Kotik [b, *]

[a] Aix-Marseille Université, Centrale Marseille, CNRS, ISM2 UMR7313, Marseille 13397, France
[b] Laboratory of Biotransformation, Institute of Microbiology of the Czech Academy of Sciences, v. v. i., The Czech Academy of Sciences, Vídeňská 1083, CZ-142 20 Prague, Czech Republic

ARTICLE INFO

Article history:
Received 4 November 2015
Received in revised form
16 December 2015
Accepted 17 December 2015
Available online 20 December 2015

Keywords:
Catalytic mechanism
Epoxide hydrolase
Electrophilic catalysis
Enantioselectivity
Fluorescence quenching
Tyrosine ionization

ABSTRACT

A detailed kinetic study based on steady-state and pre-steady-state measurements is described for the highly enantioselective epoxide hydrolase Kau2. The enzyme, which is a member of the α/β-hydrolase fold family, preferentially reacts with the (*S*,*S*)-enantiomer of *trans*-stilbene oxide (TSO) with an *E* value of ~200. The enzyme follows a classical two-step catalytic mechanism with formation of an alkyl-enzyme intermediate in the first step and hydrolysis of this intermediate in a rate-limiting second step. Tryptophan fluorescence quenching during TSO conversion appears to correlate with alkylation of the enzyme. The steady-state data are consistent with (*S*,*S*) and (*R*,*R*)-TSO being two competing substrates with marked differences in k_{cat} and K_M values. The high enantiopreference of the epoxide hydrolase is best explained by pronounced differences in the second-order alkylation rate constant (k_2/K_S) and the alkyl-enzyme hydrolysis rate k_3 between the (*S*,*S*) and (*R*,*R*)-enantiomers of TSO. Our data suggest that during conversion of (*S*,*S*)-TSO the two active site tyrosines, Tyr^{157} and Tyr^{259}, serve mainly as electrophilic catalysts in the alkylation half-reaction, polarizing the oxirane oxygen of the bound epoxide through hydrogen bond formation, however, without fully donating their hydrogens to the forming alkyl-enzyme intermediate.

1. Introduction

Epoxide hydrolases (EHs) catalyze the opening of the epoxide ring in a substrate by the addition of water, generating a diol as the final reaction product. Specifically, enantioselective or enantioconvergent EHs have found their way into various biotransformations as valuable biocatalysts [1–3]. Kau2 is a metagenome-derived EH and a member of the α/β-hydrolase fold family [4]. It turned out to be an interesting catalyst, often exhibiting a high enantiopreference (represented by a high *E* value) and/or enantioconvergence in conjunction with low product inhibition [4,5]. The enzyme has been used in a number of preparative-scale conversions with substrate loads of up to 80 g l^{-1} [4,5]. As an example, the enzyme reacted with racemic *trans*-stilbene oxide (**1**) in a highly enantioselective manner with an *E* value of ~200, resulting in the formation of *meso*-hydrobenzoin (**2**) and residual (*R*,*R*)-**1** with an *ee* of >99% in isolated yields close to the theoretical maximum of 50% (Fig. 1) [5]. (*R*,*R*)-**1** and **2** are interesting organic intermediates which have found applications as starting materials in various syntheses [6–10]. These valuable properties of the Kau2 EH prompted us to analyze its catalytic mechanism of the enantioselective hydrolysis of **1** in more detail. Moreover, kinetic data on the hydrolysis of **1** have been accumulated for the structurally related potato EH, whose enantioselectivity was shown to be low for this compound [11].

The catalytic mechanism of α/β-hydrolase fold EHs is known to involve the action of a catalytic triad, which consists of a nucleophile (Asp), a general base (His) and an acid (carboxylate function of Asp or Glu) [12]. After substrate binding to the enzyme, the nucleophilic carboxylic acid of Asp is polarized by the His–acid charge-relay system; the activated nucleophile then makes an attack on the epoxide, resulting in the formation of a covalent intermediate with an ester bond between the carboxylic acid of the

Abbreviations: A_{295}, absorbance at 295 nm; *E*, enantiomeric ratio; EH, epoxide hydrolase; TSO, *trans*-stilbene oxide.

* Corresponding author.
E-mail address: kotik@biomed.cas.cz (M. Kotik).

http://dx.doi.org/10.1016/j.abb.2015.12.008
0003-9861/

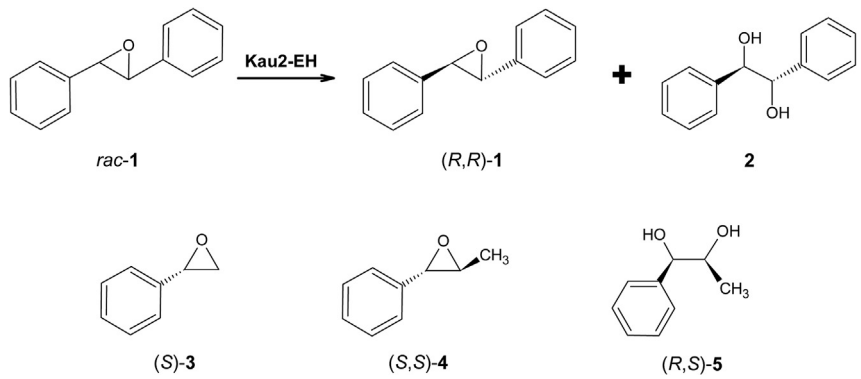

Fig. 1. Kau2 EH-catalyzed hydrolysis of racemic *trans*-stilbene oxide (**1**), and other epoxide and diol compounds used in this work. Kinetic resolution of racemic **1** results in the formation of (*R*,*R*)-**1** and *meso*-hydrobenzoin (**2**). (*S*)-styrene oxide: (*S*)-**3**; (*S*,*S*)-*trans*-1-phenyl-1,2-epoxypropane: (*S*,*S*)-**4**; (*R*,*S*)-1-phenylpropane-1,2-diol: (*R*,*S*)-**5**.

nucleophile and a carbon atom of the opened oxirane. This ester is formed in the so-called alkylation half-reaction and is termed the alkyl-enzyme intermediate; its formation appears to be associated with the observed tryptophan fluorescence quenching when rapidly mixing EH and substrate [13,14]. As a next step in the kinetic mechanism, the alkyl-enzyme intermediate is hydrolyzed, which is usually rate-limiting. In this so-called hydrolytic half-reaction the His–acid charge-relay system activates a water molecule which attacks the carbonyl of the alkyl-enzyme ester. After hydrolysis the diol product is released with the enzyme being restored to its original form (Fig. 2). There is substantial evidence that the catalytic triad is assisted by two conserved active site tyrosines. The orientation of their hydroxyl groups in crystal structures of EHs indicates an involvement of these residues in the polarization of the epoxide oxygen prior to the hydrolysis of the C–O bond [12]. Specifically, it was proposed that one of the two conserved tyrosines would establish a hydrogen bond with the epoxide oxygen of the bound substrate and thereby enhance its polarization (Fig. 2); in a consecutive step a proton transfer from the tyrosine hydroxyl to the generated alkoxide (alkyl-enzyme intermediate) would occur [12]. Recently, it was suggested that one more conserved histidine residue, which is linked to the general base histidine through the hydrolytic water molecule in the active site of the potato EH, plays a significant role in EH catalysis [15].

Several issues concerning the EH catalytic mechanism are still controversial, including the role of the two active site tyrosines. Questions to be asked in this respect are: Are tyrosinate ions being transiently formed during catalysis? Do these tyrosines serve as a general acid catalyst or as an electrophilic catalyst where no complete proton transfer to the transiently formed alkoxide intermediate occurs? In this paper we analyzed the kinetics of the conversion of **1** catalyzed by the Kau2 EH using steady-state and pre-steady-state measurements with the objective to untangle the kinetic basis of the very high enantiopreference of this enzyme and the catalytic role of its active site tyrosines during the enzymatic hydrolysis.

2. Materials and methods

2.1. Chemicals

N-cyclohexyl-*N*′-decylurea (CDU) and *N*-cyclohexyl-*N*′-(4-iodophenyl)urea (CIU) were synthesized as previously described [16,17]. The racemic compound **1**, the *meso*-diol **2**, and (*S*)-styrene oxide ((*S*)-**3**) (Fig. 1) were purchased from Sigma–Aldrich. Enantiopure (*S*,*S*)-**1** and (*R*,*R*)-**1** were obtained by preparative chiral HPLC from *rac*-**1** using a Chiralpak IC column (Daicel Corp.). (*S*,*S*)-*trans*-1-phenyl-1,2-epoxypropane ((*S*,*S*)-**4**) (Fig. 1) was synthesized as previously described [18]. (*R*,*S*)-1-phenylpropane-1,2-diol ((*R*,*S*)-**5**) (Fig. 1) was obtained by preparative kinetic resolution of *rac*-**4**

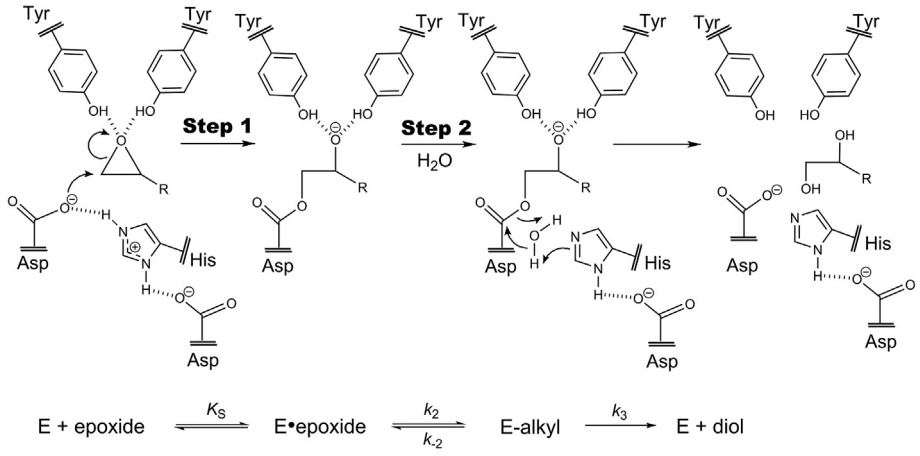

Fig. 2. Catalytic mechanism of α/β-hydrolase fold EHs. Usually, catalytic reaction mechanisms of EHs with α/β-hydrolase folds are represented by three steps: (1) formation of an enzyme–substrate complex with an equilibrium dissociation constant K_S; (2) nucleophilic attack of the active-site Asp results in the reversible formation (k_2, k_{-2}) of a covalent alkyl-enzyme intermediate (E-alkyl); (3) the enzyme intermediate is irreversibly hydrolyzed (k_3) by a base-activated water molecule, which leads to the release of the diol product.

[4].

2.2. Construction of mutants

The Kau2 EH-encoding gene was PCR-amplified using the *PfuUltra* II Fusion HS DNA polymerase (Agilent Technologies), the TOPO-cloning primers (Table S1), and the pSEKau2 plasmid as the template [4]. The PCR products were gel-purified and used for cloning into the expression vectors pET100/D-TOPO and pET101/D-TOPO (Invitrogen). Enzyme variants were generated by using either the Phusion site-directed mutagenesis kit (Thermo Fisher Scientific Inc.) or the QuickChange Lightning site-directed mutagenesis kit (Agilent Technologies) according to the manufacturers' instructions. The primers used for mutagenesis are shown in Table S1. *E. coli* BL21 Star (DE3) cells (Life Technologies) were transformed with the generated plasmids whose inserts were verified by sequencing.

2.3. Enzyme production and purification

The *E. coli* cells harboring the pET100-based plasmids were grown at 28 °C for 24 h in 5 ml of Luria Bertani medium containing 200 μg ml^{-1} of ampicillin. These cells were used to inoculate 500 ml of Terrific Broth medium containing 200 μg ml^{-1} of ampicillin. When the OD^{600} reached a value of ~1, the cultivation temperature was reduced from 37 to 23 °C, and IPTG was added (final concentration: 1.0 mM). After 4–5 h the biomass was harvested by centrifugation, frozen in liquid nitrogen and stored at −80 °C. The cells were resuspended in binding buffer (see below) in the presence of a protease inhibitor cocktail (Sigma–Aldrich) and subsequently broken in one shot using a TS Series cell disruptor (Constant Systems Ltd.) at a disruption pressure of 1300 bar. The soluble fraction of the lysate, which was obtained by centrifugation (15,500 × *g* at 4 °C, 30 min), was loaded on a Ni Sepharose column (HisTrap HP, 5 ml; ÄKTA 900 FPLC system; GE Healthcare Life Sciences) equilibrated with binding buffer (20 mM sodium phosphate, 500 mM NaCl, 30 mM imidazole, pH 7.4). The column was washed with binding buffer, and the bound Kau2 EH was eluted with a linear gradient of elution buffer (20 mM sodium phosphate, 500 mM NaCl, 500 mM imidazole, pH 7.4) using a flow rate of 3 ml min^{-1} and a gradient time of 30 min (Fig. S1). The purity of the enzymes was estimated to be >95% (Fig. S2). A HiTrap Desalting column (5 ml; GE Healthcare Life Sciences) was used for buffer exchange of the enzyme sample. Protein concentrations of the purified wild-type Kau2 EH were determined at 280 nm with a NanoDrop 2000c spectrophotometer (Thermo Scientific) using a calculated molar extinction coefficient of 58,900 M^{-1} cm^{-1} (determined using the ProtParam tool of ExPASY, http://www.expasy.org/). One unit of Kau2 EH activity is defined as the amount of enzyme necessary to hydrolyze 1 μmol of (*S*,*S*)-**1** per min in 100 mM phosphate buffer (pH 8.0) containing 4% acetonitrile (v/v) at 23 °C.

2.4. Difference spectra and determination of global pK_a for Tyr

Difference spectra were recorded between 250 and 350 nm using a UV-1700 spectrophotometer (Shimadzu Corp.). The following buffers (100 mM) were used: phosphate in the pH range 7.0–8.0; borate for the pH range 8.0–9.0, and glycine for the pH range 9.0–10.5. The concentration of tyrosinate was determined at 295 nm using Δε of 2400 M^{-1} cm^{-1} [19].

2.5. Steady-state kinetics

Initial velocity measurements were performed according to [20] by following the conversion of compound **1** to the diol **2** at 228 nm using a Cary 50 Bio UV–visible spectrophotometer (Agilent Technologies). The contents of the cuvette (2.0 ml) were continuously stirred using a tiny magnetic bar. A quadratic equation was found to best describe the relationship between absorbance and the (*S*,*S*)-**1** concentration (0–100 μM) at 30 °C in the presence of 1% acetonitrile (v/v) (Fig. S3). An extinction coefficient of 16,865 M^{-1} cm^{-1} was determined for (*S*,*S*)-**1** at 23 °C in 100 mM phosphate buffer (pH 8.0) containing 4% acetonitrile (v/v) (Fig. S4). Under both reaction conditions an extinction coefficient of 650 M^{-1} cm^{-1} was determined for **2**. All solutions containing an epoxide were freshly prepared in flasks made of glass. K_M and k_{cat} values for (*S*,*S*)-**1** were calculated from initial velocity measurements using the Michaelis–Menten equation. The specificity constant for (*R*,*R*)-**1** ($k_{cat,R}/K_{M,R}$) was calculated using the following relationship [21]:

$$E = \frac{k_{cat,S}}{K_{M,S}} \Big/ \frac{k_{cat,R}}{K_{M,R}} \tag{1}$$

The initial velocity data from experiments with reaction mixtures containing the two competing substrates (*S*,*S*)-**1** and (*R*,*R*)-**1** were analyzed using the following relationships; see [22] for Eq. (2), and [23,24] for Eq. (3):

$$\frac{v_S}{v_R} = \frac{k_{cat,S}\, K_{M,R}}{k_{cat,R}\, K_{M,S}} \frac{[S]}{[R]} \tag{2}$$

$$v_t = \frac{(k_{cat,R}/K_{M,R})\,[R] + (k_{cat,S}/K_{M,S})\,[S]}{1 + [R]/K_{M,R} + [S]/K_{M,S}} \tag{3}$$

where v_t is the total initial rate, [S] and [R] are the concentrations of (*S*,*S*)-**1** and (*R*,*R*)-**1**, and v_S and v_R are the partial reaction rates for (*S*,*S*)-**1** and (*R*,*R*)-**1**, respectively.

2.6. Pre-steady-state kinetics

Rapid mixing experiments were conducted on a SFM-300 stopped-flow apparatus (Bio-Logic Science Instruments SAS, France) equipped with 3 independently controlled syringes and 2 Ball–Berger mixers. The Trp residues were excited at 290 nm and the total fluorescence emission was detected through a 320-nm cutoff filter. All experiments were performed in 100 mM phosphate buffer (pH 8.0) containing either 1 or 4% acetonitrile at 30 or 23 °C, respectively. For each ligand concentration in the observation cell a separate manually prepared stock solution was used without changing the ligand/enzyme mixing ratio in the apparatus. Usually, 5 traces were recorded and averaged before fitting. The same instrument was used for detecting the absorbance signal at 295 nm. The stopped-flow fluorescence signal was fitted to a single exponential using

$$F = A\, e^{-k_{obs} t} + C \tag{4}$$

where *A* is the amplitude, k_{obs} is the observed rate constant, and *C* is the floating end point.

2.7. Computational ligand docking and molecular dynamics simulations

Computational docking experiments were performed using a modified version of the original Autodock program, implemented in YASARA (dock_run.mcr macro). A previously constructed homology model of the Kau2 EH was used [17]. The structures of the substrate molecules were generated in ChemDraw Ultra 9.0 and energy-minimized in Chem3D Pro 9.0. Free rotation of the

hydrogen-bonding OH groups in both oxirane-polarizing tyrosines was allowed during substrate docking. The selection of appropriately bound epoxide conformers was based on the presence of hydrogen bonds with the oxirane-polarizing tyrosines (Tyr^{157} and/or Tyr^{259}) and a proper orientation of the oxirane ring, allowing attack of the nucleophilic aspartate (Asp^{109}) at either carbon atom of the epoxide moiety. Molecular dynamics simulations were performed in a water box using YASARA (version 14.7.17) and the YAMBER3 force field. The epoxide ring of the docked (*S*,*S*)-**1** enantiomer was manually opened at the C1–O bond; then, a new covalent bond between the C1 carbon atom and the oxygen atom (located near His^{316}) of the catalytic Asp^{109} was generated. The md_refine.mcr macro was run in the 500-ps simulations at 25 °C and pH 7.4 using a water density of 0.997 g l^{-1}; one pdb file of the ligand–protein complex was saved every 25 ps.

3. Results

3.1. Solubility and photostability of compound *1*

We started our kinetic experiments using published reaction conditions (1% acetonitrile and 30 °C) [25]. A quadratic equation was found to best describe the non-linear relationship between absorbance at 228 nm and the (*S*,*S*)-**1** concentration (0–100 μM), suggesting limited solubility of this compound (Fig. S3). Moreover, samples of **1** with concentrations of >100 μM appeared to be opalescent, confirming its limited solubility (Fig. S4). To improve the solubility of **1** we modified the experimental conditions and increased the acetonitrile concentration to 4%; in addition, we lowered the reaction temperature to 23 °C to improve the long-term stability of the Kau2 EH. Under these conditions, a perfect linear relationship between the absorbance and the concentration of **1** within 0–100 μM was observed (Fig. S5).

The photostability of **1** was assessed by following the absorbance at 228 nm in the absence of enzyme using the stopped-flow apparatus (Fig. S6). It turned out that the absorbance signal decreased with time as a function of the light intensity, suggesting photolability of this compound. However, no time-dependence of the absorbance signal at 228 nm was detected in the spectrophotometer used for steady-state measurements (data not shown).

3.2. Steady-state kinetics

The Kau2 EH converted *rac*-**1** enantioselectively with (*S*,*S*)-**1** being the preferred substrate; we determined in the spectroscopic activity test a >300 times higher enzyme activity in the presence of (*S*,*S*)-**1** compared with (*R*,*R*)-**1**. The hardly detectable enzyme activity with (*R*,*R*)-**1** precluded a direct determination of any steady-state parameters for this compound. Nevertheless, the k_{cat}/K_M value for (*R*,*R*)-**1** could be estimated using the k_{cat}/K_M value obtained for (*S*,*S*)-**1** and the previously determined *E* value for the kinetic resolution of **1** (Eq. (1); Table 1) [5]. Not surprisingly, an increase in reaction temperature resulted in a higher k_{cat} value for (*S*,*S*)-**1**, whereas a lower K_M value was determined under the high-temperature conditions (Table 1).

Further, we performed initial velocity measurements with mixtures of (*R*,*R*)-**1** and (*S*,*S*)-**1** and analyzed the data using Eq. (2). As shown in Fig. S7 the (*R*,*R*)-**1**-specific reaction rate v_R was found to be low compared to the (*S*,*S*)-**1**-specific reaction rate v_S, being only 1% of v_S under conditions of a two-fold excess of (*R*,*R*)-**1** over (*S*,*S*)-**1**. The low v_R is a consequence of the high *E* value for the Kau2 EH reacting with *rac*-**1**. These initial velocity data were also analyzed using Eq. (3) with the determined k_{cat} and K_M values for (*S*,*S*)-**1**, and the estimated k_{cat}/K_M value for (*R*,*R*)-**1** (Table 1). In these simulations a good agreement between experimental velocity data and simulated curves was obtained with K_M for (*R*,*R*)-**1** being equal to 150 μM, when allowing for parameter variation within the margins of the experimental error (Fig. 3). Hence the initial velocity data determined in the presence of (*R*,*R*)-**1** and (*S*,*S*)-**1** are consistent with (*R*,*R*)-**1** and (*S*,*S*)-**1** being competing substrates for the active site of the Kau2 EH with a three-fold difference in K_M values between (*R*,*R*)-**1** and (*S*,*S*)-**1**.

Table 1
Steady-state kinetic parameters for the hydrolysis of (*S*,*S*)-**1** or (*R*,*R*)-**1** catalyzed by the Kau2 EH.

Conditions	Substrate	K_M (μM)	k_{cat} (s^{-1})	k_{cat}/K_M (μM^{-1} s^{-1})
23 °C, 4% CH_3CN	(*S*,*S*)-TSO	45 ± 4	12 ± 1	0.27 ± 0.05
	(*R*,*R*)-TSO	150[a]	0.21[a]	0.0014[b]
30 °C, 1% CH_3CN	(*S*,*S*)-TSO	15 ± 1	14 ± 1	0.93 ± 0.15
	(*R*,*R*)-TSO	n.d.	n.d.	0.0047[b]

n.d.: not determined.
[a] Estimated from simulations using Eq. (3).
[b] Estimated value using $E = 200$ and Eq. (1).

3.3. Rapid kinetics of (*S*,*S*)-*1* conversion

Multiple-turnover experiments were performed with 10–90 μM of (*S*,*S*)-**1** under conditions used for the determination of the steady-state parameters. The recorded fluorescence traces followed a single exponential curve with the apparent rate constants (k_{obs}) being linearly dependent on the (*S*,*S*)-**1** concentration (Fig. 4). Eq. (5) describes the non-linear substrate concentration ([S]) dependence of k_{obs} of a three-step reaction model (Fig. 2):

$$k_{obs} = \frac{k_2[S]}{[S] + K_S} + k_{-2} + k_3 \quad (5)$$

The observed linear relationship of k_{obs} with (*S*,*S*)-**1** implies that enzyme saturation occurred at substrate concentrations of ≫ 90 μM, indicating a high K_S value. Therefore, the data of k_{obs} *versus* (*S*,*S*)-**1** concentration was fitted to the simplified Eq. (6):

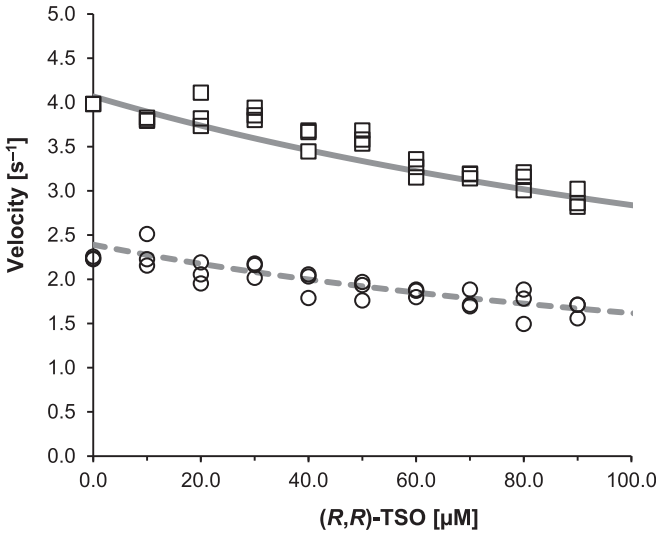

Fig. 3. Initial velocity experiments with reaction mixtures containing (*S*,*S*)-**1** and (*R*,*R*)-**1**. The concentration of (*R*,*R*)-**1** was varied between 0 and 90 μM in the presence of either 10 μM (○) or 20 μM (*S*,*S*)-**1** (□). Reaction conditions: 100 mM phosphate buffer (pH 8.0) with 4% acetonitrile, 23 °C; 60 nM Kau2 EH. The curves are based on simulations using Eq. (3) with the following input parameters: 0.29 and 0.0014 μM^{-1} s^{-1} for $k_{cat,S}/K_{M,S}$ and $k_{cat,R}/K_{M,R}$, 47 and 150 μM for the (*S*,*S*)-**1** and (*R*,*R*)-**1**-based K_M values, respectively.

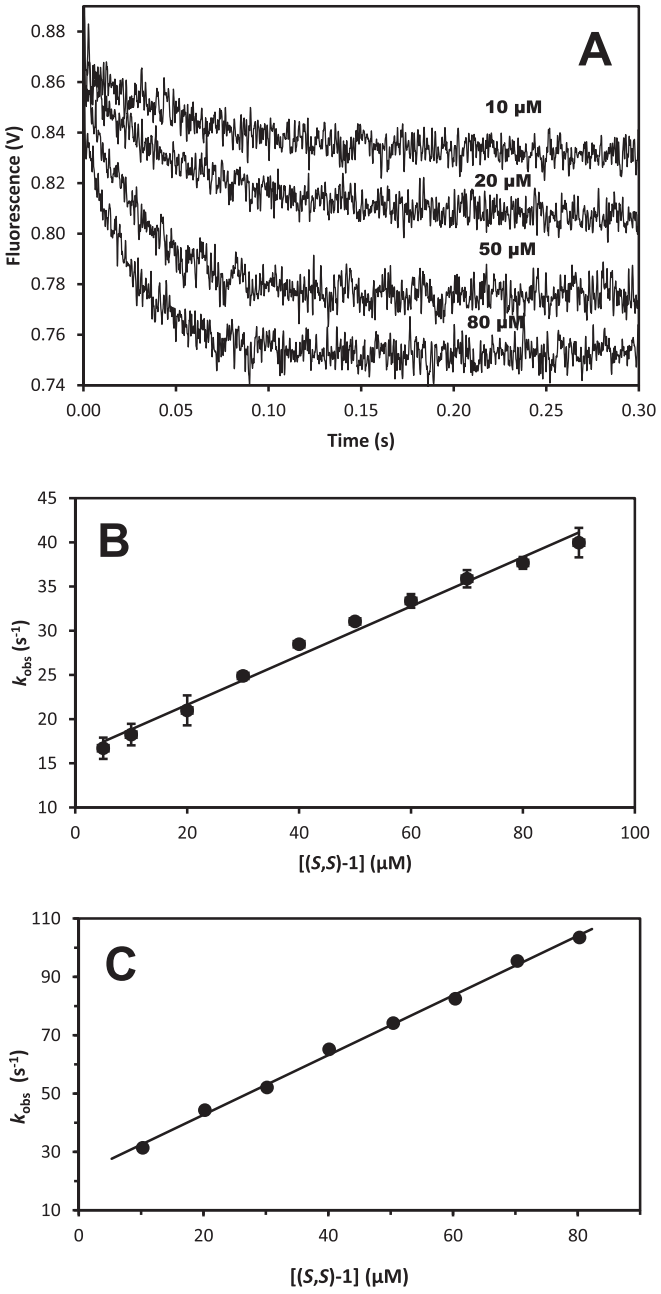

Fig. 4. Multiple-turnover experiments with different concentrations of (*S*,*S*)-**1**. (A) The fluorescence traces were recorded in the presence of 1.2 µM enzyme with 10, 20, 50, and 80 µM of (*S*,*S*)-**1** at 23 °C (pH 8.0). (B, C) Dependence of k_{obs} on the (*S*,*S*)-**1** concentration; the fits to the linear Eq. (6) are shown; (B) 23 °C, pH 8.0, with 4% acetonitrile, the data are averaged from three independent experiments; (C) 30 °C, pH 8.0, with 1% acetonitrile.

$$k_{obs} = \frac{k_2[S]}{K_S} + k_{-2} + k_3 \quad (6)$$

This enabled us to determine the values for $k_{-2} + k_3$ from the intercept and k_2/K_S from the slope. The linear relationship implies that saturation of the Michaelis complex did not occur; hence a two-step process with k_2/K_S as the second-order rate constant for the formation of the alkyl-enzyme intermediate adequately describes the enzymatic reaction under the experimental conditions used (Scheme 1) [14,22]. In this two-step process k_{cat} is defined as [26,27]:

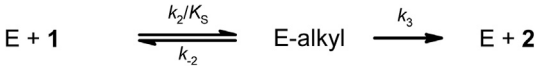

Scheme 1. Two-step reaction scheme for the Kau2 EH under the conditions used for the stopped-flow experiment.

$$k_{cat} = k_3 \quad (7)$$

Hence k_3 and k_{-2} could be calculated. Only lower limits for k_2 and K_S could be assessed (Table 2).

Additional stopped-flow experiments were performed to gain more insight into the factors responsible for the high enantiopreference of the enzyme towards (*S*,*S*)-**1**. In these experiments amplitude and k_{obs} values were found to be essentially independent of the (*R*,*R*)-**1** concentration at a fixed (*S*,*S*)-**1** concentration (Fig. S8), which suggests that the binding affinity of the enzyme for (*S*,*S*)-**1** is significantly higher than for (*R*,*R*)-**1**.

We found that the Kau2 EH was substantially photodegraded on longer time scales (1–2 s) of irradiation at 290 nm independently of the (*S*,*S*)-**1** concentration (Fig. S9). We also observed that the bleaching amplitude decreased by reducing the cosolvent (acetonitrile or ethanol) concentration. However, we did not find experimental conditions where the photodegradation would be eliminated with the substrate solubility being sufficient. We were unable to determine correct k_3 values from single-turnover experiments due to this rapid photodegrading effect and the inability to saturate the substrate with the enzyme exhibiting such a high K_S value [28].

3.4. Protein fluorescence quenching and enzyme mutants

The protein fluorescence quenching was found to be transient during conversion of (*S*,*S*)-**1**, as shown in stopped-flow experiments with the wild-type enzyme under conditions approaching single-turnovers (Fig. 5). The cause of fluorescence quenching in the wild-type Kau2 EH was investigated by constructing several enzyme variants. Replacing the nucleophile Asp^{109} by Asn or the general base His^{316} by Ala or Gln resulted in inactive enzymes with no change in their intrinsic protein fluorescence on a 400-ms time scale upon mixing them with (*S*,*S*)-**1**. These data indicate that the presence and activation of the nucleophilic carboxylic acid of Asp^{109} is required for enzyme activity and detectable quenching of the Trp fluorescence during enzymatic reaction of (*S*,*S*)-**1**.

Interestingly, mixing the wild-type Kau2 EH with either CDU or CIU, which are strong competitive disubstituted cyclohexyl urea inhibitors (K_i of 19 or 50 nM, respectively) [16,17], did not result in any detectable fluorescence quenching. As an alkyl-enzyme intermediate cannot be formed with CDU or CIU, fluorescence quenching is not observed. CDU is such a potent inhibitor that it prevents (*S*,*S*)-**1** from forming detectable amounts of an alkyl-enzyme intermediate; *i.e.* no fluorescence quenching was observed with 1.5 µM of wild-type Kau2 EH in the presence of 126 nM of CDU and 16 µM of (*S*,*S*)-**1** (data not shown).

Computational docking of (*S*,*S*)-**1** into the active site of the Kau2 EH revealed three Trp residues as possible fluorescence quenching probes: Trp^{41}, which is part of the conserved HGW/FP motif of α/β-hydrolase fold EHs; Trp^{110}, which is next to the nucleophilic Asp^{109}; and Trp^{317} being in close proximity (<3 Å) to one of the phenyl rings of bound (*S*,*S*)-**1** (Fig. 6).

Exchanging Trp^{110} for His or Ala dramatically decreased the specific activity of the enzyme from 11.5 to 0.6 or 0.1 U mg^{-1}, respectively; this indicates that mutations next to Asp^{109} can distort the orientation of the nucleophilic carboxylic acid of this residue, resulting in a profound decrease in enzyme activity.

Table 2
Determined and estimated rate constants for hydrolysis of (*S*,*S*)-**1** or (*R*,*R*)-**1** catalyzed by the Kau2 EH.

Conditions	Substrate	k_2/K_S (μM^{-1} s^{-1})	K_S (μM)	k_2 (s^{-1})	k_{-2} (s^{-1})	k_3 (s^{-1})
23 °C, 4% CH_3CN	(*S*,*S*)-TSO	0.28 ± 0.01	>1600[a]	>450[a]	3.8 ± 1.0	12.0
	(*R*,*R*)-TSO	0.0014[b]	–[c]	–[c]	<0.01[d]	0.21[d]
30 °C, 1% CH_3CN	(*S*,*S*)-TSO	1.02 ± 0.05	>1600[a]	>1600[a]	8.3 ± 1.8	14.0

[a] Estimated value considering that $K_S + [S] \approx K_S$ if $K_S > 20 \times [S]$ (see Eqs. (5) and (6); [26]).
[b] Assuming $k_{cat}/K_M = k_2/K_S$.
[c] Not assessable.
[d] Estimated values using Eqs. (7) and (8).

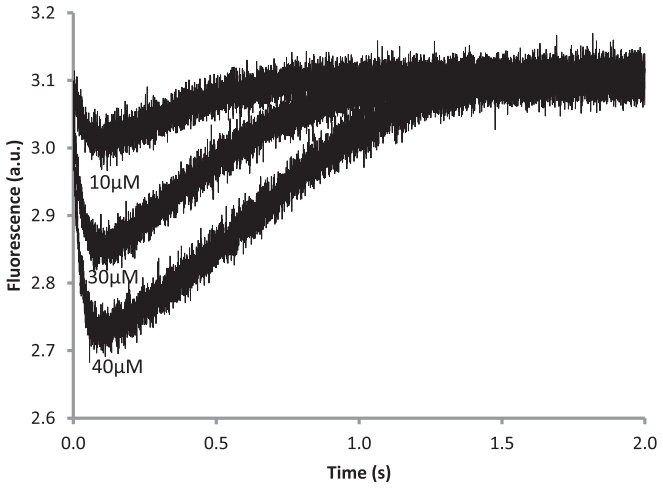

Fig. 5. Stopped-flow experiments detecting protein fluorescence. The fluorescence traces were recorded at 23 °C (pH 8.0) with 8 μM Kau2 EH and 10, 30 and 40 μM (*S*,*S*)-**1** in the presence of 1% acetonitrile.

3.5. Detection of tyrosinates

First, we intended to estimate the global pK_a value of the 9 tyrosine residues in the Kau2 EH. UV absorption spectra were recorded at different pH values between pH 7.0 and 10.5; subtracting the spectrum recorded at pH 7.0 from spectra recorded at higher pH values revealed a peak at 295 nm, which increased with pH above a pH value of 9.5. This is indicatory of tyrosinate formation [29]. From these data a global pK_a value of >10.5 was estimated (data not shown).

In an attempt to assess the possible *transient* formation of tyrosinates during the catalytic turnover of (*S*,*S*)-**1**, we recorded the absorbance at 295 nm in stopped-flow experiments and correlated this signal with fluorescence quenching data obtained under the same conditions (Fig. 7). A small build-up of the A_{295} signal was observed, which was followed by a decrease starting at ~40 ms after the mixing. The absorbance traces roughly mirrored the course of the fluorescence quenching signals. The observed decrease in the A_{295} signal appears to be determined by the concentration difference between the epoxide substrate and the diol product, which changes during the enzymatic reaction. This change in A_{295} (beyond ~40 ms) has to be explained by the depletion of the epoxide during the catalytic turnover, which *per se* leads to a decrease in absorbance at 295 nm because $\varepsilon_{epoxide} > \varepsilon_{diol}$. This substrate–product-related effect interferes with a possible enzyme-based change in the A_{295} signal. At least part of the detected small transient increase in A_{295} has to be explained by mixing artifacts; we detected such artifacts with compound **1** within the first 20–25 ms after mixing and with compound **4** within the first 10–15 ms (Figs. S10, S11, and S12). Additional control experiments were performed in the presence and absence

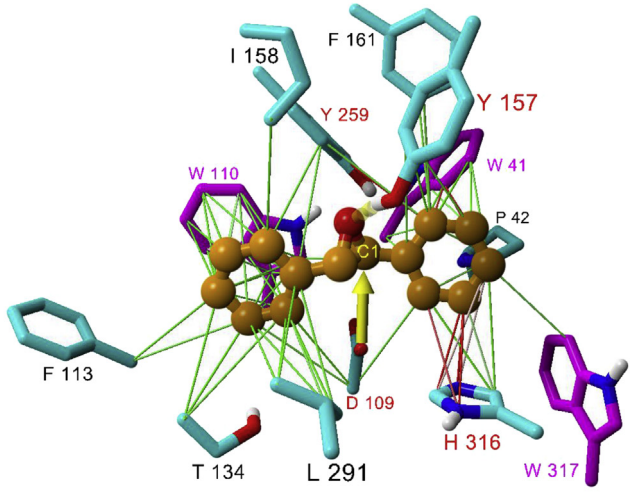

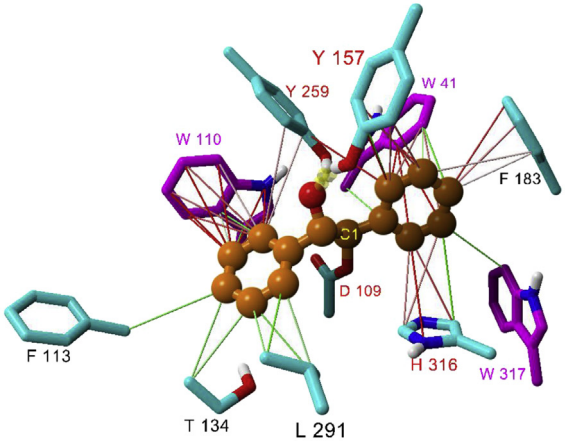

Fig. 6. View into the substrate binding pocket of the Kau2 EH homology model. The model was created by SWISS-MODEL based on the X-ray structure of murine soluble EH (1CQZ-A) [17]. The substrate (*S*,*S*)-**1** was docked into the active site (upper section) using AutoDock implemented in YASARA. The alkyl-enzyme intermediate (lower section) was constructed as described in Materials and methods and is shown after 25 ps of molecular dynamics simulation. The oxygen atoms of the epoxide and the alkyl-enzyme intermediate are positioned a hydrogen-bond distance away from both oxirane-polarizing tyrosines Tyr^{157} and Tyr^{259}. Favorable interactions stabilizing the enzyme–ligand complex or the alkyl-enzyme intermediate are depicted as green lines for hydrophobic interactions and red lines for σ–π/π–π interactions (the interaction strength is represented by shades of red, from intense red for optimal interactions to gray for minimal interactions). Only residues involved in these interactions, and the catalytically important residues Asp^{109}, His^{316}, Tyr^{157} and Tyr^{259}, and the fluorescence-generating residues Trp^{41}, Trp^{110}, and Trp^{317} are shown in stick representation. (For interpretation of the references to colour in this figure legend, the reader is referred to the web version of this article.)

of the Kau2 EH with the expectation that a fundamental difference

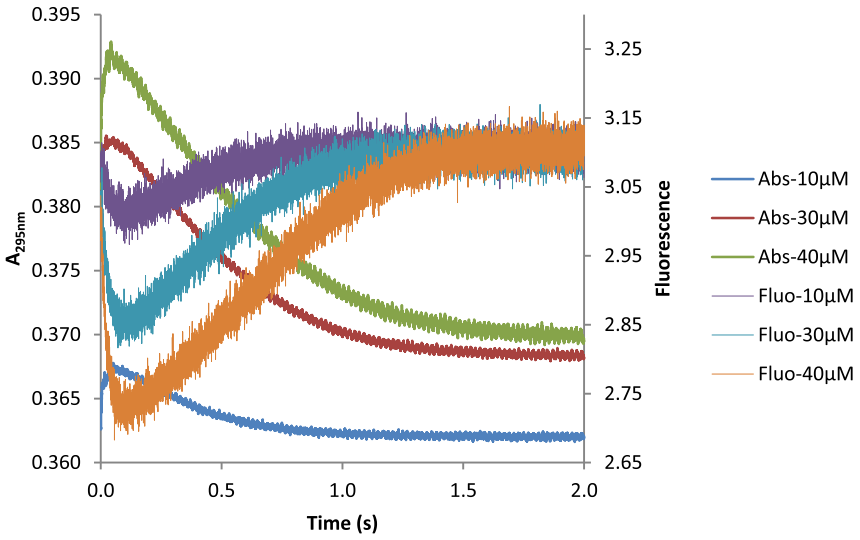

Fig. 7. Superposition of absorbance and fluorescence traces after rapid mixing of the Kau2 EH with (*S*,*S*)-**1**. Superposition of absorbance (Abs) and fluorescence (Fluo) traces recorded in the presence of 10, 30 and 40 μM (*S*,*S*)-**1** and 8 μM Kau2 EH at 1% CH_3CN and 23 °C (pH 8.0).

in the A_{295} signal would be observed between experiments with fast ((*S*,*S*)-**1** or (*S*,*S*)-**4**) and slow substrate enantiomers ((*R*,*R*)-**1** or (*R*,*R*)-**4**, Fig. S13) or between fast substrate ((*S*,*S*)-**1** or (*S*,*S*)-**4**) and product-based (**2** or (*R*,*S*)-**5**) mixing experiments. These experiments compared the A_{295} traces of the first ~30 ms after mixing where significant product formation did not yet occur in order to eliminate the substrate–product-related effect of ΔA_{295}. These controls (comparing experiments performed with and without enzyme), however, revealed that the differences in A_{295} within the first ~30 ms were small, representing not more than approximately 0.2 tyrosinate equivalents per enzyme molecule being transiently generated during conversion of (*S*,*S*)-**1** or (*S*,*S*)-**4** (assuming tyrosinate formation as the sole source of an increase in A_{295}).

4. Discussion

4.1. Kinetic mechanism and enantioselectivity

The reaction conditions which were previously described in a kinetic study of the potato EH and compound **1** served as a starting point for our experiments [25]. We then improved the solubility of **1** using modified experimental conditions, which resulted in simplified data analysis. A complication was encountered in the photodecomposition of compound **1**, which was found to interfere with the enzyme-catalyzed depletion of **1** when following the absorbance signal of **1** at 228 nm in the stopped-flow apparatus with its intense light source. As a result the enzymatic conversion of **1** cannot be monitored at 228 nm using the above-mentioned set-up of the stopped-flow apparatus. In addition, we were confronted with photodegradation of the Kau2 EH in conjunction with a high K_S value of this enzyme for (*S*,*S*)-**1**, preventing a reliable analysis of single-turnover experiments. Fast irreversible photobleaching phenomena were reported for other proteins as well [30,31].

The overall kinetic mechanism of the Kau2 EH is represented by three steps (Fig. 2); it can be simplified – under the conditions used for the stopped-flow experiments with no saturation of the (*S*,*S*)-**1**-containing Michaelis complex – to a two-step mechanism characterized by k_2/K_S, k_{-2}, and k_3 (Scheme 1). Two-step or three-step reaction mechanisms have been established for the rat liver microsomal and potato EHs depending on the substrates used [13,11]. On the other hand, an additional step representing a unimolecular isomerization of the enzyme–substrate complex had to be incorporated in the reaction scheme to adequately describe the kinetic behavior of the EH from *Agrobacterium radiobacter* AD1 with (*R*)-**3** as the substrate [26]. In all these EHs the hydrolysis of the alkyl-enzyme intermediate, which is characterized by k_3, limited the overall enzymatic reaction.

The formation of the covalent alkyl-enzyme intermediate in the Kau2 EH was found to be reversible, as with the other characterized EHs of the α/β-hydrolase fold family, with k_{-2} being smaller than k_3 by only a factor of about three (at 23 °C, 4% acetonitrile). This difference between k_{-2} and k_3 was found to be even smaller at 30 °C in the presence of 1% acetonitrile. When comparing the values for k_2 and the sum of $k_{-2} + k_3$ of both reaction conditions, it appears that accumulation of the alkyl-enzyme intermediate is more pronounced at 30 °C and 1% acetonitrile (Table 2). This accumulation of the intermediate is seen in rapid protein fluorescence quenching experiments under conditions approaching single-turnovers (Fig. 5). The accumulation of the alkyl-enzyme intermediate ($k_2 > k_3$) during conversion of (*S*,*S*)-**1** is the reason for the K_M value being markedly lower than the K_S value (45 *versus* >1600 μM). Concerning the overall kinetic mechanism with (*S*,*S*)-**1** as the substrate, the Kau2 enzyme is a standard EH with accumulation of the alkyl-enzyme intermediate and a rate-limiting hydrolysis step [13,25,26]. Interestingly, in the soybean EH, which also exhibits an α/β-hydrolase fold, the rate-limiting step of 9,10-epoxystearate conversion was deduced to be the formation of the covalent alkyl-enzyme intermediate and not its hydrolysis [32].

An *E* value of ~200 has been previously determined for the Kau2 EH-mediated kinetic resolution of **1** [5]. The factors responsible for this high enantiopreference of the enzyme were investigated by steady-state and pre-steady-state measurements. A good agreement between the k_{cat}/K_M and k_2/K_S values for (*S*,*S*)-**1** has been found (Tables 1 and 2), which indicates that the free enzyme and (*S*,*S*)-**1** were in thermodynamic equilibrium with the enzyme–substrate complex [22]. Hence the association and dissociation rates which describe the kinetics of formation of the Michaelis complex were $\gg k_2$. Assuming a similar relationship for (*R*,*R*)-**1** led to an estimation of k_2/K_S for this substrate (Table 2). Further, k_3 and k_{-2} for (*R*,*R*)-**1** could be assessed using the k_{cat} and K_M values of Table 1 and Eq. (7) in combination with Eq. (8), which defines K_M for a two-step process (Scheme 1) [26,27]:

$$K_M = \frac{K_S(k_{-2} + k_3)}{k_2} \quad (8)$$

Using these experimental and assessed data, the high enantiopreference of the Kau2 EH is best explained by pronounced differences in kinetic rate constants between the two competing substrates (*S*,*S*)-**1** and (*R*,*R*)-**1**. It appears that (*R*,*R*)-**1** is a very slow substrate with markedly lower values for the second-order alkylation rate constant (k_2/K_S) and k_3 when compared to the corresponding values for (*S*,*S*)-**1**. This is in agreement with additional stopped-flow data: (1) (*R*,*R*)-**1** altered neither the amplitude nor the k_{obs} values during the conversion of (*S*,*S*)-**1** when following enzyme fluorescence, suggesting that binding of (*R*,*R*)-**1** and its conversion to the alkyl-enzyme intermediate is severely restricted compared to (*S*,*S*)-**1**; and (2) no quenching of the enzyme fluorescence was observed in the presence of (*R*,*R*)-**1** alone, indicating that the formation of the alkyl-enzyme intermediate did not occur on a detectable level. In conclusion, the high stereospecificity of the Kau2 EH appears to be based on pronounced differences in K_M and k_{cat} values, which are best explained by marked differences in k_2/K_S and k_3 between (*S*,*S*)-**1** and (*R*,*R*)-**1**.

The factors that determine the enantioselectivity have been analyzed in other EHs; however, these EHs exhibited much lower *E* values than the one of the Kau2 EH with *rac*-**1** as the substrate. The rat liver microsomal EH was shown to have a very modest *E* value of 2 for glycidyl-4-nitrobenzoate, the enantioselectivity being chiefly controlled by k_{-2} and k_3, whose values were 10 times lower for the (*S*)-enantiomer than for the preferentially hydrolyzed (*R*)-enantiomer [13]. On the other hand, when analyzing the potato EH at pH 8.0 the determined modest selectivity for (*S*,*S*)-**1** (*E* value of 2.9) was shown to be primarily based on a slower decay reaction (k_{-2}) of the alkyl-enzyme intermediate back to the Michaelis complex [11]. Further, Rink and Janssen showed that the kinetic basis for the enantiopreference in the EH from *A. radiobacter* AD1 is mainly a large difference in alkylation rates (k_2/K_S) between (*S*)- and (*R*)-**3**, resulting in an *E* value of 16 [26]. In a rather similar manner, the very high enantiopreference of the Kau2 EH towards (*S*,*S*)-**1**, which resulted in hardly detectable enzyme activity towards (*R*,*R*)-**1**, appears to be a consequence of extensive differences in k_2/K_S and k_3 values.

4.2. Protein fluorescence quenching and enzyme mutants

The origin of the observed protein fluorescence quenching in the Kau2 EH during conversion of (*S*,*S*)-**1** appears to be linked to the transient formation of the alkyl-enzyme intermediate. An analysis of active site mutants (Asp^{109} → Asn, His^{316} → Ala/Gln, Trp^{110} → His/Ala) supports the concept that the nucleophile Asp^{109} has to be present, properly oriented, and properly activated by the general base His^{316} for a successful attack on the epoxide ring to occur. Mutations at position 110 can have a strong impact on the enzyme activity, presumably by distorting the correct position of the nucleophile Asp^{109}. It is worthwhile to note that the deleterious Ala mutation at position 110 can be overcome by introducing a second mutation at the position 113 (Gly, Arg, or Glu instead of Phe), resulting in active enzyme variants [17]. A correlation between protein fluorescence quenching and the formation of the alkyl-enzyme intermediate was also deduced from the fact that no quenching was detected within the dead-time of the instrument when mixing the Kau2 EH with (*S*,*S*)-**1**, indicating that substrate binding and formation of the Michaelis complex – taking place on a very fast time scale within the dead-time – did not cause quenching. Furthermore, a causal connection between quenching of the protein fluorescence and the formation of the alkyl-enzyme intermediate can be deduced from the absence of detectable fluorescence quenching when mixing the enzyme with the competitive inhibitors CDU or CIU, which cannot be attacked by the nucleophile Asp^{109} due to the presence of their urea NH groups [16].

A clear connection between protein fluorescence quenching and the formation of the alkyl-enzyme intermediate has been previously established for the EH from *Agrobacterium radiobacter* AD1 [26]. Drastically reduced alkylation and hydrolysis rates were reported for the potato EH variant $H^{300}N$ [25]. This is in line with our findings, which led to the conclusion that the mutation of the general base in the Kau2 EH hindered the nucleophile Asp^{109} from being properly activated, resulting in the loss of enzyme activity and the lack of detectable fluorescence quenching.

As our data suggest that significant formation of tyrosinates did not occur during the catalytic turnover of (*S*,*S*)-**1** or (*S*,*S*)-**4** (see below), the observed quenching could be explained by the build-up of the oxyanion in the alkyl-enzyme intermediate in close proximity to Trp^{41} and Trp^{110} (Fig. 6), since tryptophan fluorescence in proteins is highly dependent on the polarity of the micro-environment of this fluorophore [33]. However, we were surprised to note that (*S*)-**3**, which is a substrate of the Kau2 EH [4], did not generate any detectable protein fluorescence quenching (at (*S*)-**3** concentrations of up to 640 μM in the presence of 3.6 μM enzyme). This could be a special case explained by a change in the rate-limiting step from k_3 to k_2, which would result in no accumulation of the alkyl-enzyme intermediate. Alternatively, the smaller structure of (*S*)-**3** (compared to (*S*,*S*)-**1**) would be inadequate to generate detectable fluorescence quenching upon alkylation of the enzyme. Concerning the much bulkier epoxide (*S*,*S*)-**1**, we propose that the observed changes in Trp fluorescence are associated with changes in the micro-environment of mainly Trp^{41} and Trp^{110} caused by the transient build-up of the alkyl-enzyme intermediate generated during the enzymatic reaction. This intermediate may have its phenyl groups displaced (compared to the Michaelis complex), leading to a modification in the interaction between Trp^{41}–Trp^{110} and the bound substrate as it is converted to the transient alkyl-enzyme intermediate. See Fig. 6 for a simulation of the hydrophobic and σ–π/π–π interactions between the enzyme and (*S*,*S*)-**1** before and after the attack of the nucleophilic Asp^{109}. Molecular dynamics simulations of the alkyl-enzyme intermediate suggest a rotation of the phenyl groups after the opening of the epoxide ring, resulting in modified interaction patterns around Trp^{41} and Trp^{110} (Fig. 6).

4.3. The role of the active site Tyr^{157} and Tyr^{259}

The full role of the active site tyrosines during the EH-catalyzed conversion of the epoxide substrate is still a matter of some debate. One uncontroversial function is their involvement in the substrate binding event. As shown in several papers which analyzed active site Tyr→Phe mutants and EH–inhibitor structures [14,16,34], at least one of the active site tyrosines in EHs appears to facilitate the proper orientation of the bound epoxide by forming a hydrogen bond between the oxirane oxygen and the Tyr hydroxyl, thereby preparing it for the attack of the nucleophilic Asp.

A possible function of the active site tyrosines as proton donors has been proposed, but so far it was experimentally investigated only for the potato EH [12,35]. If these tyrosine residues were involved in a proton transfer to the transiently generated alkoxide (alkyl-enzyme intermediate), a perturbed more acidic pK_a of the Tyr-phenol group (compared to a pK_a value of 10.1 in the free amino acid; [22]) would be expected in order to facilitate the proton transfer. However, our titration data do not support the presence of tyrosine residues with unusually low pK_a values in the free enzyme; similar results were reported for the potato EH [35].

Still the possibility of a transient formation of tyrosinates during the catalytic turnover of (*S*,*S*)-**1** could not be excluded; a decrease in the pK_a of the active site Tyr residues might be brought about by transient catalytic events during conversion of the substrate. In order to examine this possibility the A_{295} was recorded in stopped-flow experiments and correlated with fluorescence quenching data. The stopped-flow traces revealed a small transient increase in A_{295} within the first 30 ms. Taking into account all the associated control experiments, we came to the conclusion that a maximum of ~0.2 tyrosinate equivalents per enzyme molecule were transiently generated during conversion of the substrate, assuming that tyrosinate formation is the sole source of an increase in A_{295}. It is important to note at this point that a transient increase in A_{295} cannot be unequivocally correlated to an increase in ionization level of tyrosines; hydrogen bonding of tryptophans or perturbations in the environment of these residues such as their transfer to a more hydrophobic medium can also result in an increase in absorbance at this wavelength [29,36–38]. As the Kau2 EH contains tryptophans and tyrosines, a proper interpretation of the small transient increase in absorbance signal upon substrate conversion has to include the possibility that it may represent not only changes in ionization level of tyrosines but also perturbations in the environment of tryptophans. Due to this ambiguity a clear-cut conclusion as to the transient formation of tyrosinates cannot be drawn; nevertheless, the data rather suggest that tyrosinate formation is not a major event in the Kau2 EH catalytic mechanism of (*S*,*S*)-**1** and (*S*,*S*)-**4** hydrolysis. We are in favor of a mechanism where complete proton transfer from the Tyr to the enzyme-bound alkoxide does not occur and transient tyrosinates are not being formed to a significant extent. The above-mentioned experiments suggest that the two conserved active site tyrosines Tyr^{157} and Tyr^{259} in the Kau2 EH serve as electrophilic catalysts [22], forming hydrogen bonds with the negatively charged alkyl-enzyme intermediate, however, without completely donating their protons to the intermediate. This is basically in line with the conclusions drawn by Elfström and Widersten for the potato EH (also containing tryptophans and tyrosines) [35], although we find their interpretation of the recorded decrease in A_{295} during the conversion of **1** problematic. They failed to mention that ΔA_{295} is strongly dependent on the concentration ratio of epoxide: diol, which is not constant during the reaction ($\Delta\varepsilon = \varepsilon_{epoxide} - \varepsilon_{diol} = 546$ or 571 M^{-1} cm^{-1} for compound **1** at pH 7.2 or 8.5, respectively). The above-mentioned mechanism implies that a water molecule – instead of the active site tyrosines – acts as the proton donor for the anionic alkyl-enzyme intermediate prior to its hydrolysis (as suggested in [35]). As an alternative, protonation of the alkyl-enzyme intermediate would be managed by one of the active site tyrosines, the immediate re-protonation of Tyr would occur through the action of a near-by water molecule [39]. Still another mechanism of Tyr re-protonation was proposed by Schiøtt and Bruice [40]; in this scenario a proton shuttle would transfer the proton of the active site base (His^{316}) to the active site Tyr and thereby prepare it for the next catalytic cycle.

The likely absence of significant tyrosinate equivalents during the EH-catalyzed conversion of compounds **1** and **4** appears not to be in contradiction with molecular dynamics simulations performed by Schiøtt and Bruice using the murine soluble EH as a model [40]. However, Hopmann and Himo concluded in their study of a small quantum-chemical model of human soluble EH using a density functional theory method that the formed alkyl-intermediate was protonated through a proton transfer from one of the two conserved active site Tyr during the conversion of **4** [41]. On the other hand, in a quantum mechanics/molecular mechanics modeling study Lonsdale and co-workers suggested that their data rather support a mechanism in which the active site tyrosines in murine soluble EH act as hydrogen bond donors and are not deprotonated during the catalytic cycle [42]. For the time being, it is unclear to what extent these theoretical studies and experimental data represent general or substrate–enzyme-specific results of EH-catalyzed reactions.

5. Conclusions

Monitoring the protein fluorescence quenching in the Kau2 EH enabled us to follow the transient formation of the alkyl-enzyme intermediate during conversion of **1**. We have shown that the Kau2 enzyme in the presence of substrate **1** reacts as a standard EH with accumulation of the alkyl-enzyme intermediate followed by a rate-limiting hydrolysis step. The kinetic data suggest that the high enantiopreference of the Kau2 EH towards **1** (*E* value of ~200) is based on marked differences in k_{cat} and K_M values between the competing substrates (*S*,*S*)-**1** and (*R*,*R*)-**1**. Further, the extensive enantioselectivity of the EH is best explained by profound differences in the second-order alkylation rate constant (k_2/K_S) and k_3 for the two enantiomers of **1**. Our data do not support the presence of significant tyrosinate equivalents during the enzymatic hydrolysis of epoxides **1** and **4**. Thus it appears that the active site Tyr^{157}–Tyr^{259} pair does not serve as a proton donor to the transiently formed alkoxide enzyme intermediate during the alkylation half-reaction; the active site tyrosines rather serve as electrophilic catalysts, polarizing the oxygen of the bound epoxide through (a) hydrogen bond(s), thereby facilitating the opening of the epoxide ring.

Acknowledgments

We are grateful to Jalila Simaan (Aix-Marseille University) for her help with the stopped-flow apparatus. In addition, we thank Marion Jean and Nicolas Vanthuyne (Aix-Marseille University) for their preparative chiral HPLC experiments. In addition, we are indebted to Elise Courvoisier-Dezord (Platform AVB, Aix-Marseille University) for her help in the bioreactor manipulations. This work was partially supported by the Academy of Sciences of the Czech Republic (grant F-13-14-05) and the CNRS (France). We also acknowledge support from the Institute of Microbiology of the Academy of Sciences of the Czech Republic (RVO61388971).

Appendix A. Supplementary data

Supplementary data related to this article can be found at http://dx.doi.org/10.1016/j.abb.2015.12.008.

References

[1] A. Archelas, R. Furstoss, Synthetic applications of epoxide hydrolases, Curr. Opin. Chem. Biol. 5 (2001) 112–119.
[2] A. Steinreiber, K. Faber, Microbial epoxide hydrolases for preparative biotransformations, Curr. Opin. Biotechnol. 12 (2001) 552–558.
[3] M. Kotik, A. Archelas, R. Wohlgemuth, Epoxide hydrolases and their application in organic synthesis, Curr. Org. Chem. 16 (2012) 451–482.
[4] M. Kotik, V. Štěpánek, M. Grulich, P. Kyslík, A. Archelas, Access to enantiopure aromatic epoxides and diols using epoxide hydrolases derived from total biofilter DNA, J. Mol. Catal. B Enzym. 65 (2010) 41–48.
[5] W. Zhao, M. Kotik, G. Iacazio, A. Archelas, Enantioselective bio-hydrolysis of various racemic and *meso* aromatic epoxides using the recombinant epoxide hydrolase Kau2, Adv. Synth. Catal. 357 (2015) 1895–1908.
[6] Nugent W.A. (2001), Catalysts for asymmetric addition of organozinc reagents to aldehydes and method for preparation. US Patent 6187918 B1.
[7] S. Florio, V. Aggarwal, A. Salomone, Lithiation and reactions of stilbene oxides: synthetic utility, Org. Lett. 6 (2004) 4191–4194.
[8] K. Bica, P. Gaertner, Application of *meso*-hydrobenzoin-derived chiral auxiliaries for the stereoselective synthesis of highly substituted pyrrolidines by 1,3-dipolar cycloaddition of azomethine ylides, Tetrahedron Asymmetry 21 (2010) 641–646.
[9] T. Arai, K. Sakagami, Asymmetric benzoylation of *meso*-hydrobenzoin using a reusable tripodal imidazoline–pyridine–Cu catalyst, Eur. J. Org. Chem. 2012

(2012) 1097–1100.
[10] M. Torres-Werlé, A. Nano, A. Maisse-François, S. Bellemin-Laponnaz, Asymmetric benzoylation and Henry reaction using reusable polytopic bis(oxazoline) ligands and copper(II), New J. Chem. 38 (2014) 4748–4753.
[11] D. Lindberg, A. Gogoll, M. Widersten, Substrate-dependent hysteretic behavior in StEH1-catalyzed hydrolysis of styrene oxide derivatives, FEBS J. 275 (2008) 6309–6320.
[12] C. Morisseau, B.D. Hammock, Epoxide hydrolyses: mechanisms, inhibitor designs, and biological roles, Annu. Rev. Pharmacol. Toxicol. 45 (2005) 311–333.
[13] H.-F. Tzeng, L.T. Laughlin, S. Lin, R.N. Armstrong, The catalytic mechanism of microsomal epoxide hydrolase involves reversible formation and rate-limiting hydrolysis of the alkyl–enzyme intermediate, J. Am. Chem. Soc. 118 (1996) 9436–9437.
[14] R. Rink, J. Kingma, J.H. Lutje Spelberg, D.B. Janssen, Tyrosine residues serve as proton donor in the catalytic mechanism of epoxide hydrolase from *Agrobacterium radiobacter*, Biochemistry 39 (2000) 5600–5613.
[15] B.A. Amrein, A. Bauer, F. Duarte, Naworyta A. Carlsson Å.J., S.L. Mowbray, M. Widersten, S.C.L. Kamerlin, Expanding the catalytic triad in epoxide hydrolases and related enzymes, ACS Catal. 5 (2015) 5702–5713.
[16] M.A. Argiriadi, C. Morisseau, M.H. Goodrow, D.L. Dowdy, B.D. Hammock, D.W. Christianson, Binding of alkylurea inhibitors to epoxide hydrolase implicates active site tyrosines in substrate activation, J. Biol. Chem. 275 (2000) 15265–15270.
[17] M. Kotik, W. Zhao, G. Iacazio, A. Archelas, Directed evolution of metagenome-derived epoxide hydrolase for improved enantioselectivity and enantioconvergence, J. Mol. Catal. B Enzym. 91 (2013) 44–51.
[18] S. Pedragosa-Moreau, A. Archelas, R. Furstoss, Microbiological transformations 32: use of epoxide hydrolase mediated biohydrolysis as a way to enantiopure epoxides and vicinal diols: application to substituted styrene oxide derivatives, Tetrahedron 52 (1996) 4593–4606.
[19] A.N. Glazer, The chemical modification of proteins by group-specific and site-specific reagents, in: H. Neurath, R.L. Hill (Eds.), The Proteins, Volume 2, third ed., Academic Press, New York, 1976, 1–103.
[20] L.S. Hasegawa, B.D. Hammock, Spectrophotometric assay for mammalian cytosolic epoxide hydrolase using *trans*-stilbene oxide as the substrate, Biochem. Pharmacol. 31 (1982) 1979–1984.
[21] A.J.J. Straathof, J.A. Jongejan, The enantiomeric ratio: origin, determination and prediction, Enzyme Microb. Technol. 21 (1997) 559–571.
[22] A. Fersht, Enzyme Structure and Mechanism, second ed., W.H. Freeman and Company, New York, USA, 1985.
[23] M. Dixon, E.C. Webb, Enzymes, second ed., Longmans, Green and Co. Ltd., London, UK, 1964.
[24] T. Pocklington, J. Jeffery, Competition of two substrates for a single enzyme, Biochem. J. 112 (1969) 331–334.
[25] L.T. Elfström, M. Widersten, Catalysis of potato epoxide hydrolase, StEH1, Biochem. J. 390 (2005) 633–640.
[26] R. Rink, D.B. Janssen, Kinetic mechanism of the enantioselective conversion of styrene oxide by epoxide hydrolase from *Agrobacterium radiobacter* AD1, Biochemistry 37 (1998) 18119–18127.
[27] A. Cornish-Bowden, Fundamentals of Enzyme Kinetics, third ed., Portland Press Ltd., London, 2004, p. 48.
[28] K.A. Johnson, Enzyme Kinetics: Transient Phase. in: ELS, John Wiley & Sons Ltd, Chichester, 2005. http://www.els.net.
[29] S.N. Timasheff, Some physical probes of enzyme structure in solution, in: P.D. Boyer (Ed.), The Enzymes, Volume II, third ed., Academic Press, New York and London, 1970, pp. 371–442.
[30] H.-H. Kim, Y.M. Lee, J.-K. Suh, N.W. Song, Photodegradation mechanism and reaction kinetics of recombinant human interferon-α2a, Photochem. Photobiol. Sci. 6 (2007) 171–180.
[31] F. Rivardo, T.G.H. Leach, C.S. Chan, T.M.L. Winstone, C.L. Ladner, K.J. Sarfo, R.J. Turner, Unique photobleaching phenomena of the twin-arginine translocase respiratory enzyme chaperone DmsD, Open Biochem. J. 8 (2014) 1–10.
[32] E. Blée, S. Summerer, M. Flenet, H. Rogniaux, A. Van Dorsselaer, F. Schuber, Soybean epoxide hydrolase, J. Biol. Chem. 280 (2005) 6479–6487.
[33] A.B.T. Ghisaidoobe, S.J. Chung, Intrinsic tryptophan fluorescence in the detection and analysis of proteins: a focus on Förster resonance energy transfer techniques, Int. J. Mol. Sci. 15 (2014) 22518–22538.
[34] T. Yamada, C. Morisseau, J.E. Maxwell, M.A. Argiriadi, D.W. Christianson, B.D. Hammock, Biochemical evidence for the involvement of tyrosine in epoxide activation during the catalytic cycle of epoxide hydrolase, J. Biol. Chem. 275 (2000) 23082–23088.
[35] L.T. Elfström, M. Widersten, Implications for an ionized alkyl-enzyme intermediate during StEH1-catalyzed *trans*-stilbene oxide hydrolysis, Biochemistry 45 (2006) 205–212.
[36] D. Freifelder, Physical Biochemistry, Applications to Biochemistry and Molecular Biology, second ed., W.H. Freeman and Company, San Francisco, USA, 1982.
[37] E.H. Strickland, C. Billups, E. Kay, Effects of hydrogen bonding and solvents upon the tryptophanyl ^1L_a absorption band. Studies using 2,3-dimethylindole, Biochemistry 11 (1972) 3657–3662.
[38] K.J. Rothschild, P. Roepe, P.L. Ahl, T.N. Earnest, R.A. Bogomolni, S.K. Das Gupta, C.M. Mulliken, J. Herzfeld, Evidence for a tyrosine protonation change during the primary phototransition of bacteriorhodopsin at low temperature, Proc. Natl. Acad. Sci. U. S. A. 83 (1986) 347–351.
[39] M. Widersten, A. Gurell, D. Lindberg, Structure–function relationships of epoxide hydrolases and their potential use in biocatalysis, Biochim. Biophys. Acta Gen. Subj. 1800 (2010) 316–326.
[40] B. Schiøtt, T.C. Bruice, Reaction mechanism of soluble epoxide hydrolase: insights from molecular dynamics simulations, J. Am. Chem. Soc. 124 (2002) 14558–14570.
[41] K.H. Hopmann, F. Himo, Theoretical study of the full reaction mechanism of human soluble epoxide hydrolase, Chem. Eur. J. 12 (2006) 6898–6909.
[42] R. Lonsdale, S. Hoyle, D.T. Grey, L. Ridder, A.J. Mulholland, Determinants of reactivity and selectivity in soluble epoxide hydrolase from quantum mechanics/molecular mechanics modeling, Biochemistry 51 (2012) 1774–1786.